ADVANCES IN ATMOSPHERIC SCIENCES, VOL. 33, DECEMBER 2016, 1361–1375

Modulation of Tropical Cyclogenesis in the Western North Pacific by the Quasi-Biweekly Oscillation

Haikun ZHAO*[1], Chunzai WANG[2], and Ryuji YOSHIDA[3]

[1]*Key Laboratory of Meteorological Disaster, Ministry of Education/Joint International Research Laboratory of Climate and Environment Change/Collaborative Innovation Center on Forecast and Evaluation of Meteorological Disaster/Pacific Typhoon Research Center/Earth System Modeling Center, Nanjing University of Information Science and Technology, Nanjing* 210044*, China*

[2]*NOAA/Atlantic Oceanographic and Meteorological Laboratory, Miami, FL,* 33149*, USA*

[3]*RIKEN Advanced Institute for Computational Science, Kobe,* 650-0047*, Japan*

(Received 19 December 2015; revised 27 May 2016; accepted 13 June 2016)

ABSTRACT

The quasi-biweekly oscillation (QBWO) is the second most dominant intraseasonal mode over the western North Pacific (WNP) during boreal summer. In this study, the modulation of WNP tropical cyclogenesis (TCG) by the QBWO and its association with large-scale patterns are investigated. A strong modulation of WNP TCG events by the QBWO is found. More TCG events occur during the QBWO's convectively active phase. Based on the genesis potential index (GPI), we further evaluate the role of environmental factors in affecting WNP TCG. The positive GPI anomalies associated with the QBWO correspond well with TCG counts and locations. A large positive GPI anomaly is spatially correlated with WNP TCG events during a life cycle of the QBWO. The low-level relative vorticity and mid-level relative humidity appear to be two dominant contributors to the QBWO-composited GPI anomalies during the QBWO's active phase, followed by the nonlinear and potential intensity terms. These positive contributions to the GPI anomalies are partly offset by the negative contribution from the vertical wind shear. During the QBWO's inactive phase, the mid-level relative humidity appears to be the largest contributor, while weak contributions are also made by the nonlinear and low-level relative vorticity terms. Meanwhile, these positive contributions are partly cancelled out by the negative contribution from the potential intensity. The contributions of these environmental factors to the GPI anomalies associated with the QBWO are similar in all five flow patterns—the monsoon shear line, monsoon confluence region, monsoon gyre, easterly wave, and Rossby wave energy dispersion associated with a preexisting TC. Further analyses show that the QBWO strongly modulates the synoptic-scale wave trains (SSWs) over the WNP, with larger amplitude SSWs during the QBWO's active phase. This implies a possible enhanced (weakened) relationship between TCG and SSWs during the active (inactive) phase. This study improves our understanding of the modulation of WNP TCG by the QBWO and thus helps with efforts to improve the intraseasonal prediction of WNP TCG.

Key words: tropical cyclogenesis, quasi-biweekly oscillation, genesis potential index, large-scale patterns, western North Pacific

Citation: Zhao, H. K., C. Z. Wang, and R. Yoshida, 2016: Modulation of tropical cyclogenesis in the western North Pacific by the quasi-biweekly oscillation. *Adv. Atmos. Sci.*, **33**(12), 1361–1375, doi: 10.1007/s00376-016-5267-z.

1. Introduction

The western North Pacific (WNP) is the most active region for tropical cyclogenesis (TCG) worldwide. On average, there are about 26 tropical cyclones (TCs) generated over the WNP each year (Chan, 2005). These TCs often cause casualties and damage to property over East Asia and adjacent regions (Zhang et al., 2009). Over the WNP, the variability of TC activity can be found on various time scales, including interdecadal or decadal (Ho et al., 2004; Chan, 2008; Liu and Chan, 2008; Zhao et al., 2014; Zhao et al., 2014; Zhao and Wang, 2015), interannual (Lander, 1994; Chia and Ropelewski, 2002; Wang and Chan, 2002; Camargo and Sobel, 2005; Zhao et al., 2010, 2011), and intraseasonal time scales (Liebmann et al., 1994; Wang and Zhou, 2008; Camargo et al., 2009; Wang et al., 2009; Huang et al., 2011; Li and Zhou, 2013a, 2013b; Zhao et al., 2015a, 2015b). Considering the potential societal impacts and scientific significance of TC activities, a better understanding of TC activities in the WNP and their variabilities are important and necessary.

On the intraseasonal time scale, the MJO (Madden and

* Corresponding author: Haikun ZHAO
Email: zhk2004y@gmail.com

Julian, 1971) is considered to be the dominant mode, with a period of about 30–60 days. The MJO can modulate changes in environmental conditions and thus lead to a clustering of TC formation during the TC season (Gray, 1979). The general consensus is that the MJO has a strong impact on TCG events globally, with more TCs formed during its convectively active phase in comparison with that during convectively suppressed phases (Gray, 1979; Camargo et al., 2009; Klotzbach, 2014; Klotzbach and Oliver, 2015). Over the WNP, a prominent north-northeastward movement of the MJO during boreal summer has been widely documented (Yasunari, 1979; Hsu et al., 2004; Jiang et al., 2004; Yoshida et al., 2014; Zhao et al., 2015a, 2015b). Along with the propagation of the MJO, the location of WNP TCG shifts correspondingly and the number of TCs increases (reduces) during active (inactive) phases of the MJO (Liebmann et al., 1994; Kim et al., 2008; Huang et al., 2011; Li and Zhou, 2013a; Wu and Duan, 2015; Zhao et al., 2015a, 2015b).

Most studies have focused on the impact of the MJO on WNP TC activity. Meanwhile, the modulation of TC activity by the quasi-biweekly oscillation (QBWO) has been relatively less well studied. The QBWO over the WNP during boreal summer tends to move northwestward, with a prevailing period of 10–30 days, as identified in many previous studies (e.g., Li and Zhou, 1995; Wang et al., 2009; Chen and Sui, 2010; Li and Zhou, 2013a; Zhao et al., 2015a). Some studies have suggested that the QBWO can strongly affect Indian and Asian monsoon rainfall (Chen and Chen, 1993; Chang and Chen, 1995; Wang and Xu, 1997; Chen et al., 2000) and local TC activity (Hartmann et al., 1992; Wang et al., 2009; Li and Zhou, 2013a, 2013b; Zhao et al., 2015a). Moreover, Li and Zhou (1995) found that the kinetic energy of the QBWO over the WNP is much stronger than that of the MJO. We also computed the standard deviations of rainfall based on TRMM Product 3B42 data (Huffman et al., 2007), for the peak TC season (May–October), 1998–2012, in both the 10–30-day and 30–60-day bands (figure not shown). The results showed the variance of rainfall anomalies in the 10–30-day band to be stronger than that in the 30–60-day band, which is consistent with previous studies (Li and Zhou, 1995; Zhao et al., 2015a). Meanwhile, the high frequency of WNP TC occurrence matches well with vigorous QBWO activity, implying a possible link between the QBWO and WNP TCG. In a recent study, Li and Zhou (2013a) examined the relationship between the QBWO and TCG over the WNP basin by qualitatively investigating changes in environmental factors modulated by the QBWO. However, the impacts of these large-scale environmental parameters on WNP TCG have not been quantitatively assessed. Additionally, although TCG is closely associated with large-scale conditions (Gray, 1968; McBride and Zehr, 1981), how different large-scale conditions modulate TCG over the WNP basin remains unclear.

Ritchie and Holland (1999) subjectively identified the five basic large-scale patterns [i.e., the monsoon shear line (SL), monsoon confluence region (CF), monsoon gyre (GY), easterly wave (EW), and Rossby wave energy dispersion associated with a preexisting TC (PTC)] favorable for WNP TCG. In order to overcome the subjectivity of these five patterns, Yoshida and Ishikawa (2013) developed an objective algorithm for identifying the five flow patterns. Many studies have illustrated that the two leading intraseasonal oscillation modes over the WNP, i.e., the MJO and QBWO, can distinctly modulate WNP TCG events (Kim et al., 2008; Wang et al., 2009; Huang et al., 2011; Wu et al., 2011; Li and Zhou, 2013a; Zhao et al., 2015a, 2015b). However, studies on the modulation of these two dominant intraseasonal oscillation modes, and their association with different flow patterns, remain very limited. Recently, Zhao et al. (2015b) investigated the impact of the MJO on WNP TCG and its association with the five large-scale patterns mentioned above, but the QBWO's modulation of WNP TCG and its link to the flow patterns were not quantitatively assessed in their study.

As an extension to Zhao et al. (2015b), the modulation of TCG by the QBWO, and its association with the aforementioned five large-scale patterns, are investigated in this study. One of the main objectives of this work is to explore the relative importance of environmental factors associated with the five flow patterns in their impacts on TCG. In addition to the well-recognized impacts of these environmental factors on TCG that have been discussed in previous studies (Gray, 1968; McBride and Zehr, 1981; Klotzbach and Gray, 2008; Dare and McBride, 2011), synoptic-scale wave trains (SSWs) aligned in a southeast to northwest direction, with a typical wavelength of about 2500–3000 km and a period of 3–8 days, are also regarded as a major precursor to TCG (Reed and Recker, 1971; Reed et al., 1977; Yasunari, 1979; Nakazawa, 1986, 1988; Lau and Lau, 1990; Takayabu and Nitta, 1993; Dickinson and Molinari, 2002; Li and Fu, 2006; Zhao et al., 2016). To further investigate the possible link between SSWs and the TCG associated with the five large-scale patterns, the modulation by the QBWO of the SSWs associated with the large-scale patterns is also discussed in this study.

The paper is organized as follows: Section 2 describes the datasets used in the study and the identification of the WNP QBWO mode. A diagnostic tool for investigating the relative role of large-scale factors in modulating WNP TCG is also introduced in this section. The key factors associated with the QBWO that affect TCG, and the modulation of the SSWs by the QBWO, over the WNP, are explored in section 3. Section 4 summarizes the study's key findings.

2. Datasets and methodology

2.1. *Data*

The TC data are from the JTWC best-track dataset. The peak TC season (i.e., May–October) during 1998–2012 is selected for analysis. In this study, we focus on the early stage of TCG events. Thereby, only those TCs with maximum sustained wind speed greater than or equal to 13 m s^{-1} (25 knots) are considered.

To extract the leading QBWO mode and SSWs over the WNP, we obtain rainfall observations for the period 1998–2012 from TRMM Product 3B42 (Huffman et al., 2007),

which extends from 50°S to 50°N with a 0.25° horizontal resolution and a 3-hourly temporal resolution.

To objectively identify basic large-scale patterns favorable for TCG and to explore key environmental factors associated with the QBWO that affect TCG over the WNP, 6-hourly variables including winds, relative humidity, temperature and SST are derived from JRA-25/the JMA Climate Data Assimilation System (Onogi et al., 2007).

2.2. *Methodology*

2.2.1. *Identification of the five large-scale patterns*

Following Yoshida and Ishikawa (2013), the large-scale patterns associated with all the 331 TCG cases during May–October from 1998 to 2012 are classified. The large-scale pattern with the largest normalized contribution score is referred to as the determined flow pattern for each TCG. Details on the computation of the normalized contribution score of the five patterns for each individual TCG event can be found in Yoshida and Ishikawa (2013) and Zhao et al. (2015b).

Typical examples of TCG corresponding to the five major flow patterns are obtained using the objective algorithm developed by Yoshida and Ishikawa (2013). As shown in Fig. 1a, the contribution score is highest from the SL pattern; the second largest contribution score is from the GY pattern, followed by the relatively weak contribution score from the PTC pattern. Therefore, the SL pattern is identified to be the major contribution pattern. The scores for the three patterns are shown in Fig. 1b. It can clearly be seen that the contribution score of the CF pattern is the largest, followed by that of the SL and GY patterns. Similarly, the major EW pattern can be obtained based upon the calculated contribution score shown in Fig. 2a. In Fig. 2b, only the contribution score of the GY pattern can be detected by the algorithm, while no score is computed for the other flow patterns. The major PTC pattern is presented in Fig. 3a, in which a preexisting TC and relatively weak cyclonic vorticity are observed, although the relatively weak contribution from the SL pattern can be found. Specifically, an unclassified flow pattern is displayed in Fig. 3b, with no scores for the five flow patterns of interest.

The SL appears to be the most frequent flow pattern contributing to WNP TCG. It is associated with about 42% of the 331 TCG events, followed by the CF (18%) and EW (16%) patterns. The PTC (7%) and GY (4%) patterns can be detected, but they only make small contributions to WNP TCG. The same results were found by Zhao et al. (2015b), and these results agree well with the results of previous studies (Ritchie and Holland, 1999; Yoshida and Ishikawa, 2013). Note that there are some slight differences in the percentages of TCG frequency associated with each large-scale pattern between the results of this study and that of previous studies. There are three possible reasons for these small differences. The first is the different detecting algorithms used. The second reason is different study periods covered. And the last reason is that the impact of climate change differs among different decades.

Further analyses illustrate no significant difference in TC locations over the peak season under the five large-scale patterns, except a more eastward shift in the average location of TCG associated with the PTC pattern, at the 5% confidence level.

2.2.2. *Identification of the QBWO*

Similar to previous studies (Wang et al., 2009; Li and Zhou, 2013a; Zhao et al., 2015a, 2015b), an extended EOF (EEOF) analysis is used for extracting the QBWO mode over the WNP basin. Before performing the EEOF analysis, the TRMM daily rainfall anomalies for the period 1998–2012 are filtered in the 10–30-day band. The domain (0°–30°N, 100°–160°E) is selected for the EEOF analyses. Similar to Zhao et al. (2015b), the QBWO over the WNP can be identified by the EEOF1 and EEOF2. A prevailing period of about 20 days for the two EEOF modes can be found in the time series of the principal components (PCs) of EEOF1and EEOF2 (figure not shown), in accordance with the peak period of the QBWO in previous studies (Wang et al., 2009; Li and Zhou, 2013a; Zhao et al., 2015a). The lagged regression patterns of band-pass filtered TRMM rainfall for the EEOF1 and EEOF2 modes further show a pronounced northwestward propagation for the QBWO (figure not shown), which is consistent with results in previous studies (Yasunari, 1979; Hsu et al., 2004; Wang et al., 2009; Lee et al., 2013; Li and Zhou, 2013a; Zhao et al., 2015a). In summary, the first two leading EEOF modes of the observed daily rainfall anomalies can successfully capture the dominant QBWO mode over the WNP.

Similar to previous studies (Kim et al., 2008; Li and Zhou, 2013a, Zhao et al., 2015a, 2015b), the daily QBWO amplitude and phase (ranging from 1 to 8) can be determined by the two leading EEOF PCs (i.e., PC1 and PC2) following the same method adopted in Wheeler and Hendon (2004). In this study, QBWO events are determined for days with amplitude greater than or equal to 1.0 (i.e., $\sqrt{\mathrm{PC1}^2 + \mathrm{PC2}^2} \geqslant 1.0$).

2.2.3. *Diagnostics for exploring the role of environmental factors*

The genesis potential index (GPI) (Emanuel and Nolan, 2004) is used for exploring the contribution of each individual environmental factor to TCG under all the five large-scale patterns in this study. The GPI is expressed as

$$\mathrm{GPI} = |10^5\xi|^{\frac{3}{2}} \left(\frac{H}{50}\right)^3 \left(\frac{V_{\mathrm{pot}}}{70}\right)^3 (1 + 0.1V_{\mathrm{shear}})^{-2}, \qquad (1)$$

where ξ, H, V_{pot}, and V_{shear} are the 850 hPa absolute vorticity (s^{-1}), 600 hPa relative humidity (%), potential intensity (PI) ($\mathrm{m\ s}^{-1}$), and vertical wind shear, respectively. The vertical wind shear is computed as the vector difference between the winds at 200 hPa and 850 hPa ($\mathrm{m\ s}^{-1}$). The terms $\eta = |10^5\xi|^{\frac{3}{2}}, \gamma = (H/50)^3, \varphi = (V_{\mathrm{pot}}/70)^3$, and $s = (1 + 0.1V_{\mathrm{shear}})^{-2}$ represent the four GPI components, which are associated with 850 hPa absolute vorticity, 600 hPa relative humidity, PI, and vertical wind shear, respectively. The algorithm of Bister and Emanuel (2002) is used for computing PI. In this algorithm, SST and vertical profiles of temperature and specific humidity in the troposphere are considered.

As the QBWO propagates northwestward, the anomalous

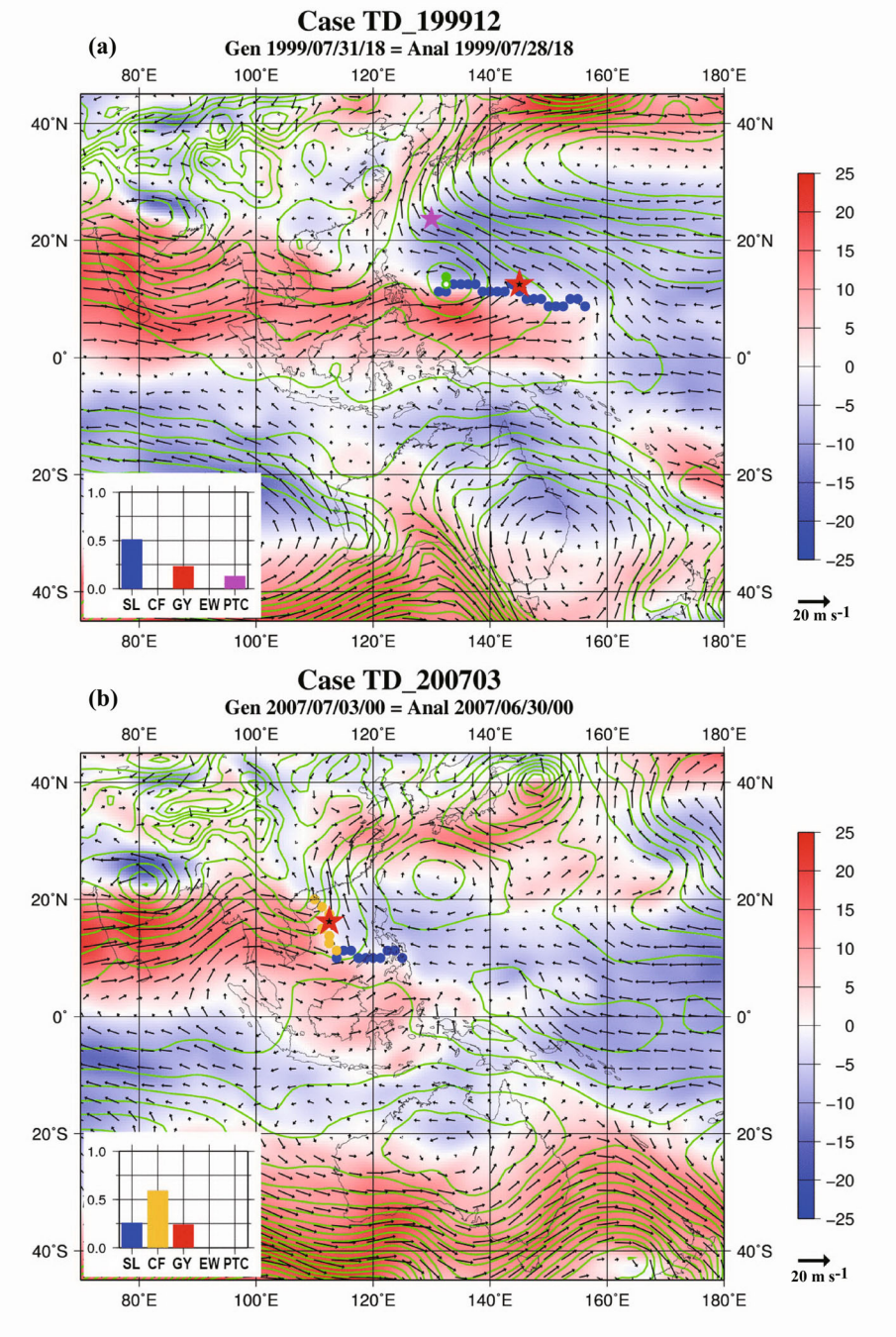

Fig. 1. Examples of (a) SL and (b) CF patterns. The red stars represent the locations of TCG. The purple stars indicate a preexisting TC about 1500 km to the west of the TCG location denoted by red stars at the genesis time. The yellow dotted line shows the detected leading edge of the westerly wind by the objective algorithm, and represents a part of the CF region. The blue dotted line indicates the shear line, which is detected near the genesis location by the objective algorithm. Vectors are the horizontal wind field at 850 hPa and the color-shaded area is the zonal wind at 850 hPa. Green contours represent SLP.

GPI patterns match well with TCG counts and shifts in genesis area, which will be shown later in section 3.1. To further understand the modulation of WNP TCG by the QBWO, we assess the respective roles of the four large-scale factors involved in the GPI [i.e., η, γ, φ and s in Eq. (1)] in contributing to the GPI anomalies, following the methodology detailed in Jiang et al. (2012).

3. TCG associated with the QBWO

3.1. *Statistical characteristics*

The composite rainfall anomalies along with TCG locations during a life cycle of the QBWO are displayed in Fig. 4. The northwestward propagating QBWO can significantly modulate WNP TCG. For example, the TCG zone exhibits

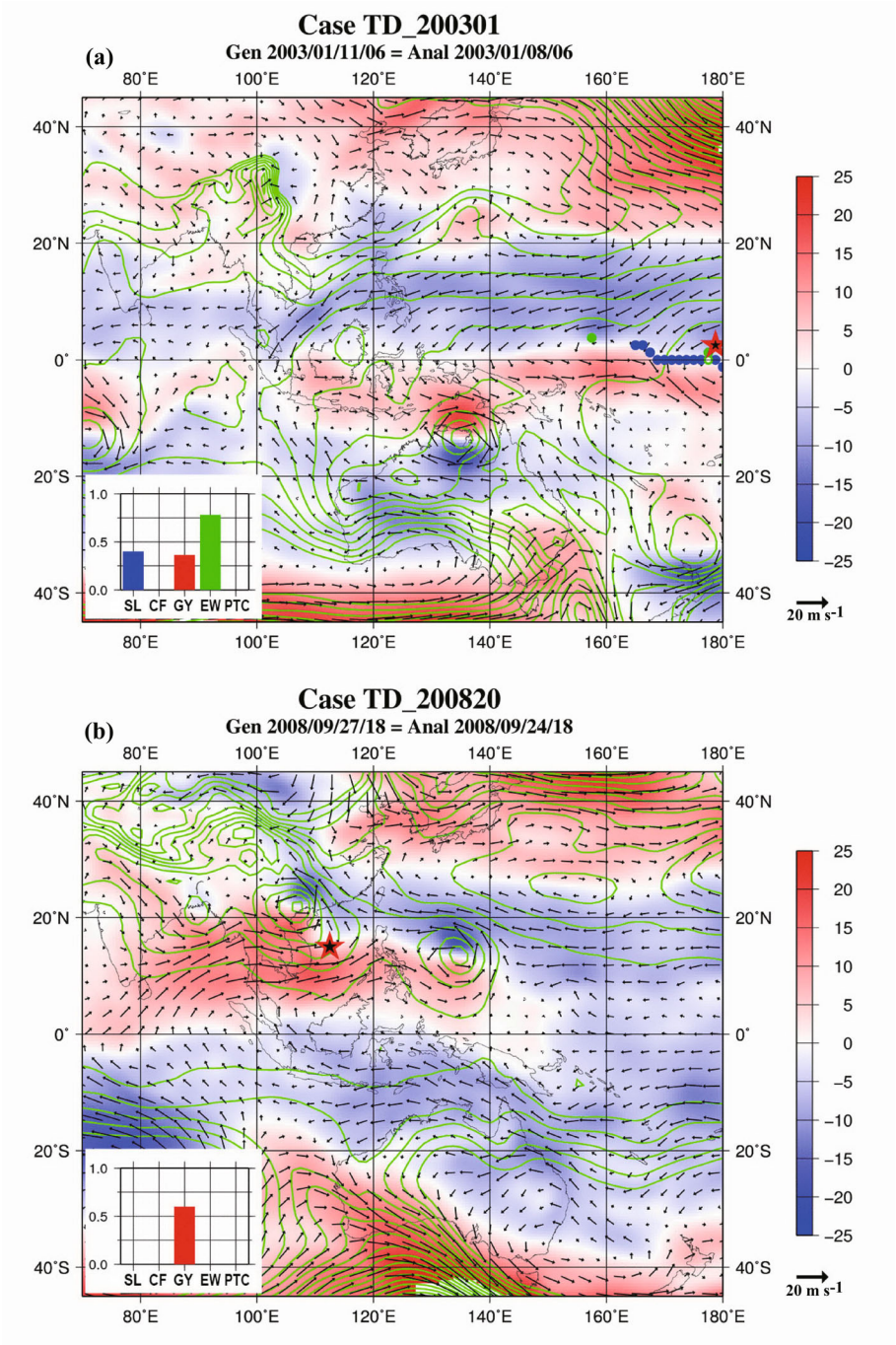

Fig. 2. As in Fig. 1 but for the (a) EW and (b) GY patterns. The green dotted line represents part of the EW trough, as detected by the objective algorithm.

a clear migration coupled with the northwestward movement of the enhanced convection from phases 1 to 4 of the QBWO. In addition to the shift in TCG locations, a strong impact of the QBWO on TCG counts can be readily seen. As shown in Fig. 5a, more TCs occur during QBWO phases 1–4 and fewer cases occur during phases 5–8, corresponding to enhanced convection over the main development region of WNP TCG in phases 1–4 and suppressed convection in phases 5–8 of the QBWO. Such a distinct modulation of WNP TCG by the QBWO mode is further indicated by the TCG rate (Fig. 5b), which is computed by the ratio of TCG counts to the number of total days. Similarly, it is readily found that the main development regions of TCG events associated with each large-scale pattern have no significant difference, except that the TCG location associated with the PTC pattern shifts more eastward in all the QBWO phases. Additionally, the CF flow pattern associated with the easternmost TCG location during phase 6 (Fig. 4) can be detected. Furthermore, the ratios of occurrence of each individual large-scale pattern during the QBWO phases are also examined. The results are almost identical to those without separating them into large-scale patterns. In all the flow patterns, except the PTC pattern,

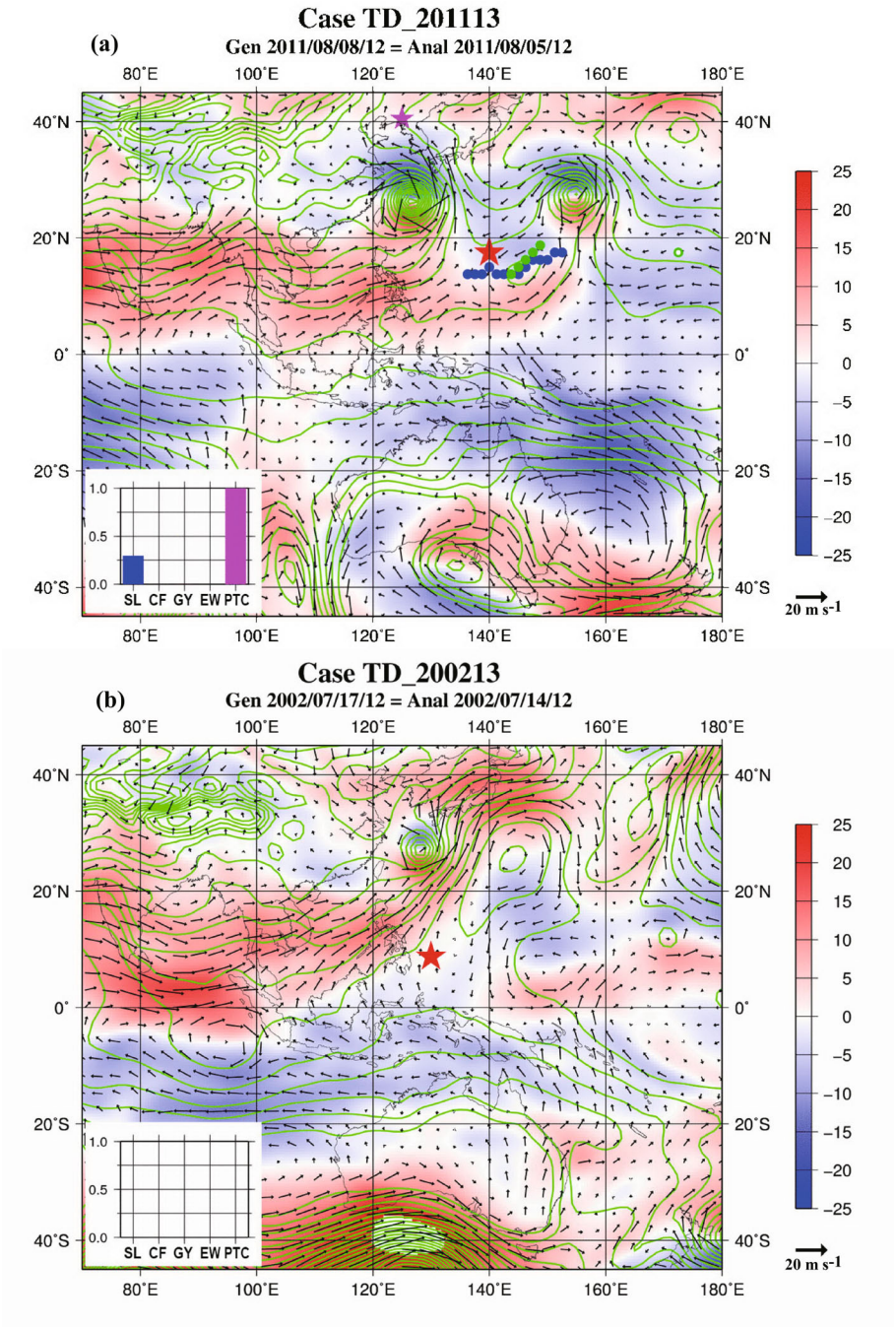

Fig. 3. As in Fig. 1 but for the (a) PTC and (b) unclassified flow patterns.

more TCG cases occur during the active phases (1–4) than during the inactive phases (5–8). It is noteworthy that slightly more TCG cases occur during the inactive phases under the PTC pattern (Fig. 6).

To have enough TCG samples and obtain more robust results, we combine phases 1–4 into one category (hereafter, the active QBWO phase) and phases 5–8 into another (hereafter, the inactive QBWO phase). Consequently, the difference in the TCG cases between the active and inactive QBWO phases becomes much clearer. 43.5% of the total number (i.e., 144) of TCG events is found in the active phase and 29.9% of the total number (i.e., 99) of TCG events is observed during the inactive phase. In summary, these results suggest a significant impact of the QBWO on TCG events over the WNP. Compared with the modulation of TCG events by the MJO, discussed in Zhao et al. (2015a), the impact of the QBWO mode on WNP TCG is weaker. This is mainly because the QBWO has a strong impact on local TC activity, while the MJO has a strong impact on basin-wide TC activity, as suggested in previous studies (Li and Zhou, 2013a; Zhao et al., 2015a).

Figure 6 further shows the TCG counts associated with the five large-scale patterns during the active and inactive QBWO phases. A more consistent modulation of WNP TCG

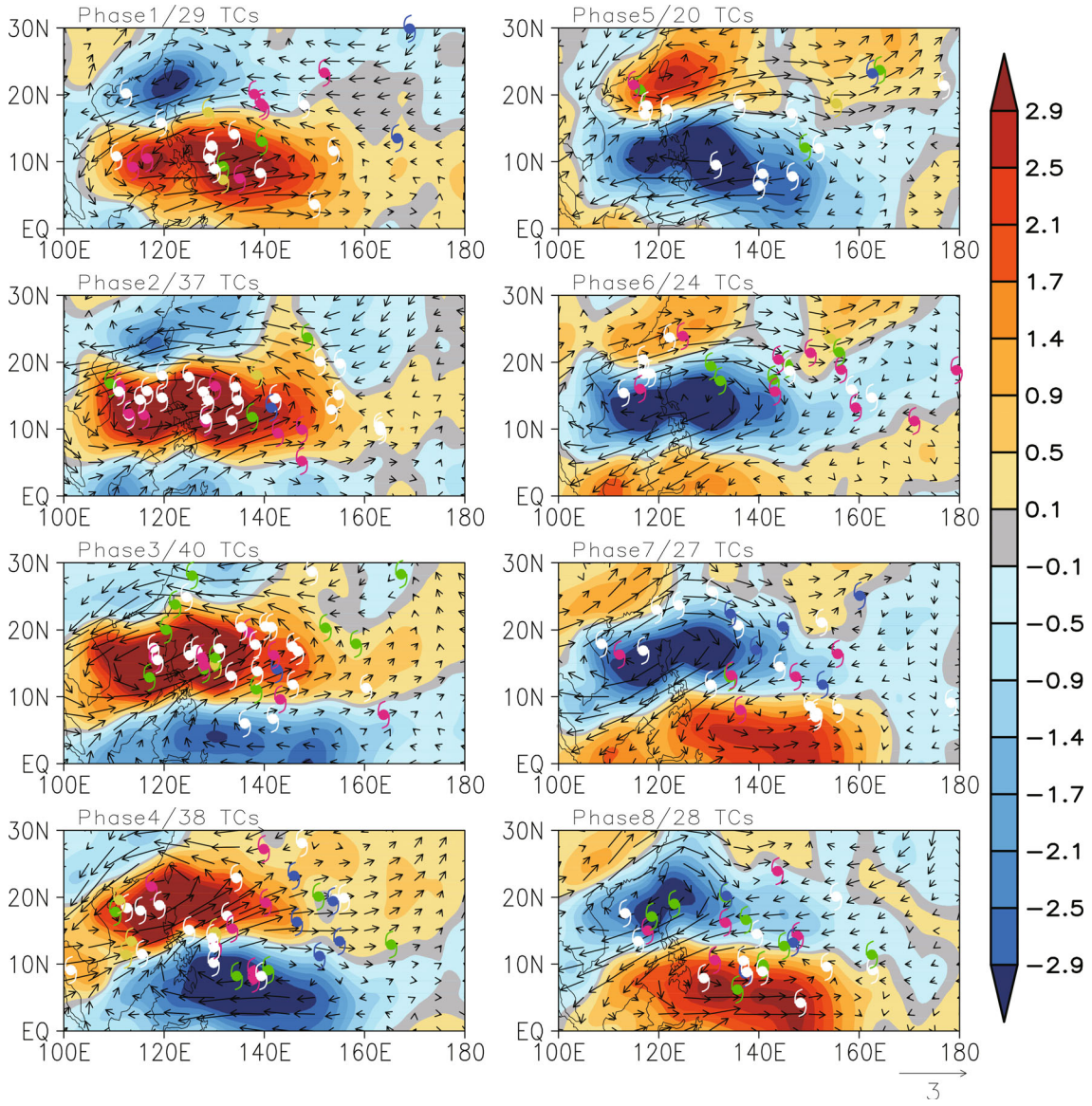

Fig. 4. Composite rainfall anomalies (color-shaded; units: mm d^{-1}) during different QBWO phases superimposed on TCG events. TCG cases associated with the SL (in white), CF (in purple), EW (in green), PTC (in blue) and GY (in yellow) large-scale patterns are given for the QBWO phases.

by the QBWO than that by the MJO is found for all five of the flow patterns (Zhao et al., 2015b). Generally, more events occur during the active QBWO phase under all five flow patterns, except the PTC pattern. Under the PTC pattern, there are slightly more TCG events during the inactive QBWO phase than that during the active QBWO phase, which may be associated with the northwestward propagation of the QBWO. These results are in agreement with the determination of the five major flow patterns. Enhanced westerly wind, and thus intensified monsoonal circulation, can be found during the active phase, resulting in more WNP TCG events associated with the three monsoon-related flow patterns (i.e., SL, CF and GY). In contrast, enhanced easterly wind anomalies, and thus a weakened monsoon trough, over the WNP, can be detected during the inactive QBWO phase, leading to fewer TCG cases under the aforementioned three monsoon-related large-scale patterns. Additionally, there are slightly more TCG cases associated with the EW flow pattern during the active QBWO phase. This may be because the easterly wind intensifies (weakens) over the northeastern side of the enhanced (weakened) monsoon trough over the WNP basin during the active (inactive) QBWO phase, and thus provides more (less) chance for TCG. Meanwhile, TCG locations associated with the EW flow pattern shift more northeastward than that associated with the other three monsoon-related large-scale patterns.

3.2. *Role of environmental factors*

Figure 7 shows the composite GPI anomalies and WNP TCG locations during the convectively active and inactive QBWO periods. Corresponding to the composite rainfall anomalies (figure not shown), the positive (negative) GPI

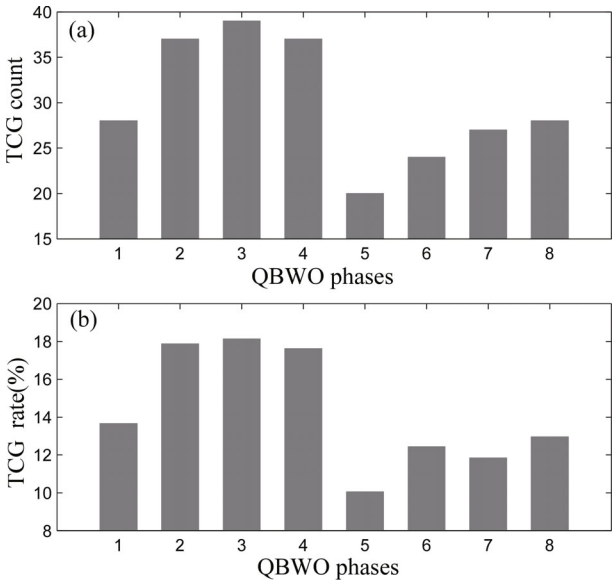

Fig. 5. The TCG (a) count and (b) rate (100× TCG count/QBWO days) during the different QBWO phases.

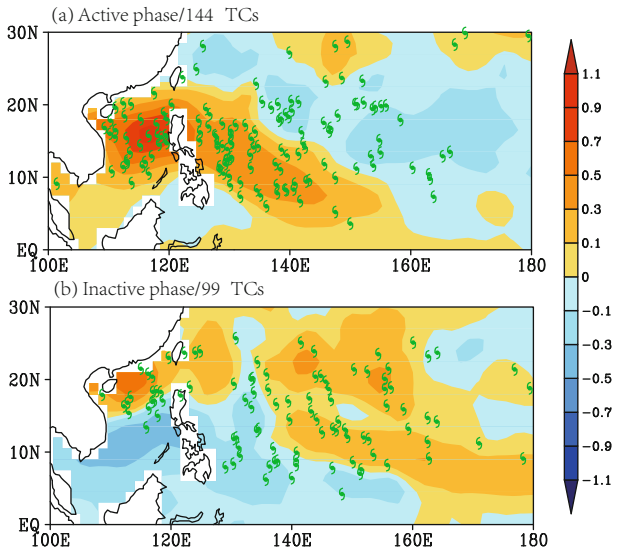

Fig. 7. Composite GPI anomalies (color-shaded) during the (a) active and (b) inactive QBWO phase along with TCG events. The green icons represent typhoon.

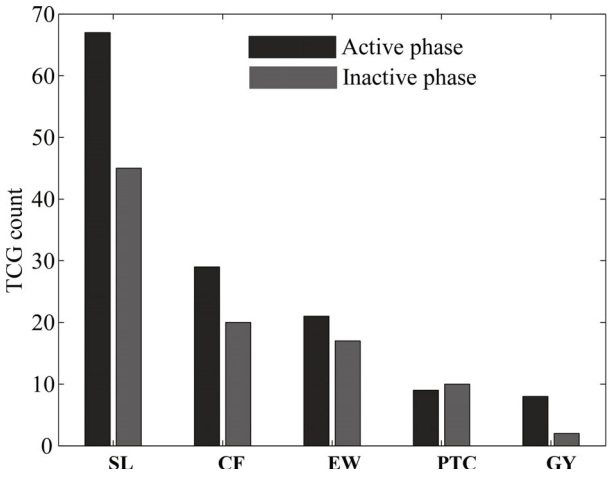

Fig. 6. TCG count associated with each of the five large-scale patterns (SL, CF, EW, PTC, GY) during the active and inactive QBWO phases.

anomalies are generally consistent with the active (inactive) phase of convection. In contrast to that during the inactive QBWO phase, enhanced TCG events can be detected in regions with positive GPI anomalies during the active phase. Furthermore, most TCG events tend to form over the monsoon region aligned in the northwest–southeast direction during the active QBWO phase, while more TCG cases occur outside the monsoon trough during the inactive phase. All of these results suggest that the QBWO plays an important role in modulating TCG by changing environmental factors. It is worth noting that a certain number of TCG events can be detected in areas of negative GPI anomalies, as shown in Fig. 7. Two possible reasons may explain this phenomenon. One is that while the GPI reduces with respect to the base state, it is still high enough to support TC genesis. The other is that other factors not included in Eq. (1) or not associated with the QBWO, such as the MJO and convectively coupled equatorial waves, may affect TCG. Further study is needed to better explore the associated physical mechanism.

The relative importance of the four factors involved in the GPI index is further investigated in this section. The spatial distributions of the four linear terms associated with the total GPI anomalies during the active and inactive phases, along with TCG events, over the WNP, are shown in Fig. 8. During the active phase, positive GPI anomalies with varying 850 hPa relative vorticity (referred to as GPI-VOR) and 600 hPa relative humidity (referred to as GPI-RH) appear to be more consistent with WNP TCG events, and the PI variation also contributes to TCG events. However, most of TCG events over the WNP are associated with negative GPI anomalies with varying vertical wind shear (referred to as GPI-Shear). In contrast to that during the active phase, the largest contribution to the total GPI anomalies during the inactive phase is from the mid-level relative humidity. Distinct from that during the active phase, the PI variation in the eastern part of the WNP (referred to as GPI-PI) makes a positive contribution to the GPI anomalies. Generally, the contributions of environmental factors to the GPI anomalies depend on the QBWO phase. During the active phase, the two leading contributions to positive GPI anomalies are from the enhanced 850 hPa relative vorticity and increased 600 hPa relative humidity, whose contributions are slightly offset by the negative contributions from the vertical wind shear. A relatively similar and small contribution from the nonlinear term (referred to as GPI-nonlinear) can be found during both active and inactive phases (Fig. 9). This is different from the case associated with the MJO mode, as indicated in Zhao et al. (2015b). The nonlinear term appears not to be a significant contributor,

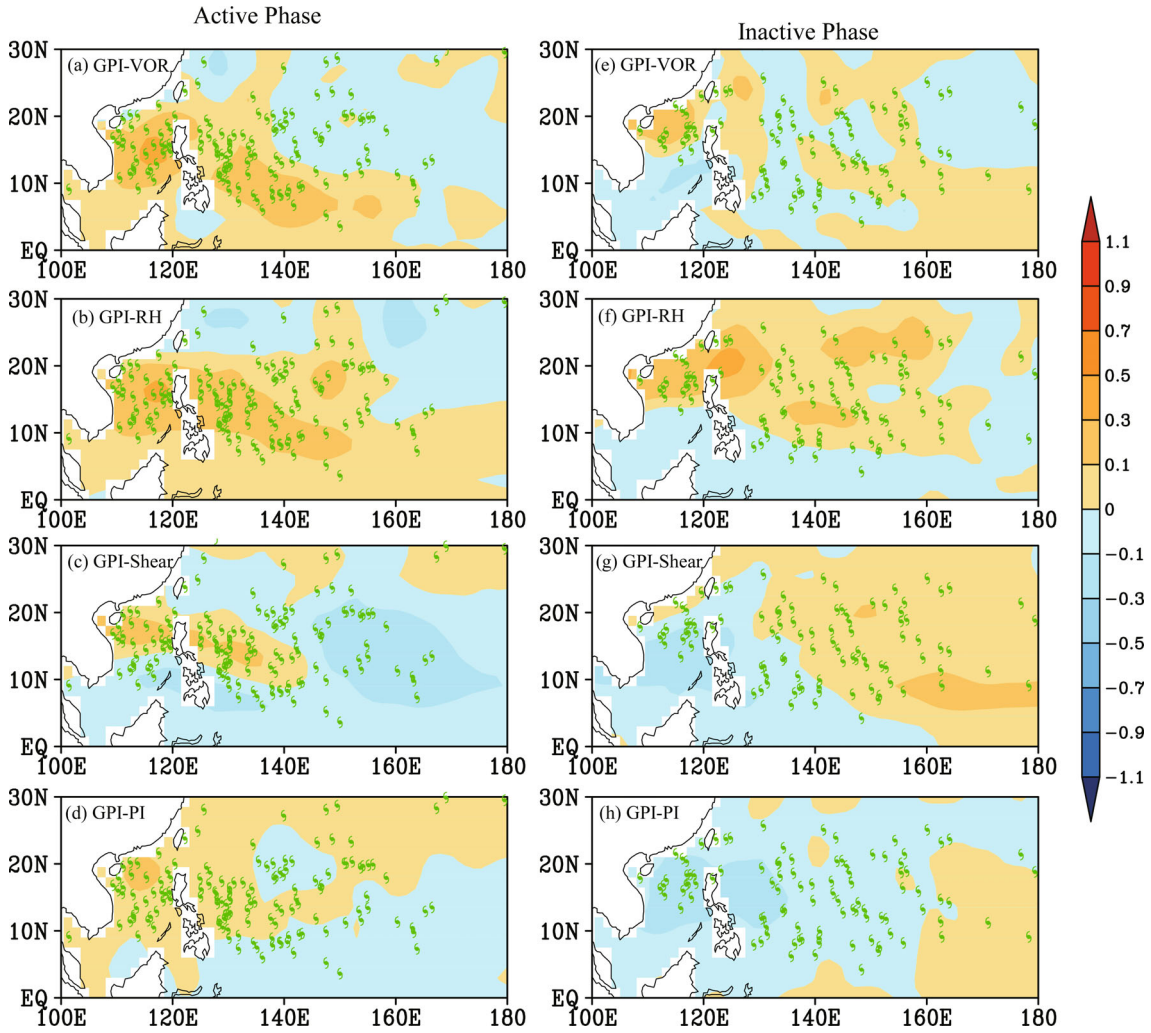

Fig. 8. Spatial distributions of the contributions of (a, e) vorticity (b, f) relative humidity, (c, g) and (d, h) potential intensity to the total GPI anomalies over the WNP during the (a–d) active and (e–h) inactive QBWO phases. The green icons represent typhoon.

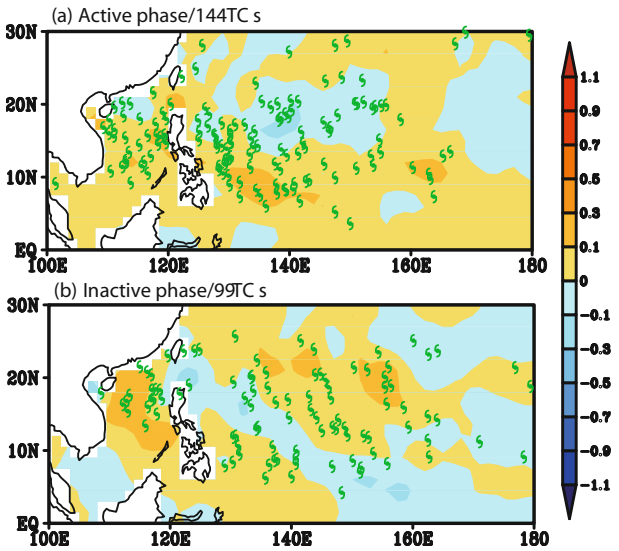

Fig. 9. Spatial distributions of the contributions of nonlinear terms to the total GPI anomalies over the WNP during the (a) active and (b) inactive phases. The green icons represent typhoon.

which is further enhanced by displaying the small composite GPI anomalies averaged within the $10^\circ \times 10^\circ$ box centered in TCG locations for all TCG cases, without separating them into large-scale patterns, during the active and inactive QBWO phases (Fig. 10).

3.3. *Impact of large-scale patterns*

In this section, similar analyses as above are conducted to assess the relative importance of environmental factors in modulating WNP TCG cases under all five flow patterns. Figure 10 shows the mean composite GPI anomalies with the $10^\circ \times 10^\circ$ domain centered on the TCG locations for all TCG cases associated with each large-scale pattern on days with and without TCGs during the active and inactive QBWO phases, respectively. The results show that a positive contribution to the GPI under all of the five large-scale flow patterns during the active phase comes mainly from two factors, i.e., 850 hPa relative vorticity and 600 hPa relative humidity. A weak positive contribution from the nonlinear and PI terms can also be found. Meanwhile, it is readily seen that the negative contribution from the vertical wind shear can partly

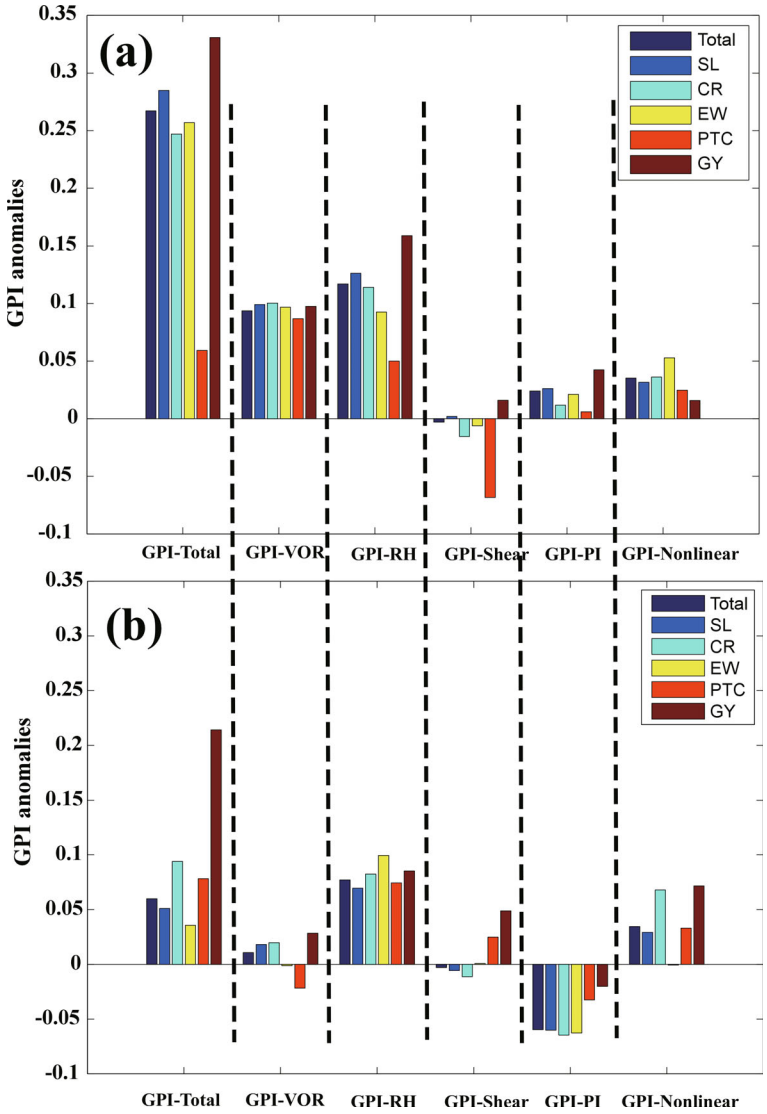

Fig. 10. Contribution of the different terms [(i.e., Vorticity, Vertical wind shear, RH, PI, and nonlinear terms] to the total GPI anomalies over the WNP during the (a) active and (b) inactive QBWO phases, for the five large-scale patterns, individually (SL, CF, EW, PTC, GY) and combined (Total).

reduce the positive contributions discussed above. These results are similar to the results from analyzing the total 331 WNP TCG cases without considering them under the five large-scale patterns, as shown in section 3.1. Specifically, the GPI anomalies associated with the GY flow pattern appear to be larger than those associated with other flow patterns, and a weak positive contribution can be found from the vertical wind shear. During the inactive phase, the mid-level relative humidity makes the most important contribution to the positive anomalies. Positive contributions can also be found from the nonlinear term and vertical wind shear, and a weak positive contribution from the 850 hPa relative vorticity. The positive contribution is largely offset by the negative contribution from the PI term. These results are also similar to the results obtained without distinguishing the large-scale patterns, except the role of vertical wind shear. During the active phase, the positive contribution to the GPI anomalies can be found from the vertical wind shear for the GY large-scale pattern, which is distinct from the result obtained without distinguishing the large-scale patterns.

Considering the possible contamination of the influence of TCs themselves on the magnitude of the GPI anomalies, the magnitude of the averaged composite GPI anomalies with the $10^\circ \times 10^\circ$ domain centered on the TCG location for all TCG cases associated with each large-scale pattern on the 1348 non-TC days is computed for the active and inactive QBWO phases, respectively. The roles of these factors in contributing to GPI anomalies is basically similar to those without excluding TC days during the active and inactive phases, although a slight difference in magnitude can be found. Therefore, the results discussed above on the importance of environmental factors in contributing to the compos-

ite GPI anomalies are robust.

3.4. *Modulation of SSWs by the QBWO*

The SSW train is one of the most frequent occurring weather patterns during boreal summer over the WNP. Many studies have suggested that SSWs actually serve as a major source for WNP TCG events (Sobel and Bretherton, 1999; Li et al., 2006; Fu et al., 2007). In this section, the modulation of SSWs by the QBWO is investigated, which sheds light on the impact of the QBWO on WNP TCG cases.

To extract the SSWs over the WNP from the data, an EEOF analysis of 3–8-day bandpass filtered TRMM rainfall is performed. Similar to the QBWO mode, the SSWs can be captured by the first two leading EOF modes, as shown in Fig. 11. The amplitude of the SSW activity can be computed as the magnitude of the two leading EEOF PCs, i.e., $\mathrm{SSW}_{\mathrm{amplitude}} = \sqrt{\mathrm{PC1}^2 + \mathrm{PC2}^2}$. Looking at the lead–lag SSW patterns, it is found that the SSWs are characterized by a northwestward propagation, with a typical wavelength of about 2500 km. To further explore the impact of the QBWO on the SSWs, the amplitude of the SSWs during the active and inactive QBWO phases is computed. The results are shown in Fig. 12. During the active QBWO phase, the SSW amplitude is about 1.50, which is stronger than the SSW amplitude 1.15 during the inactive phase. A similar and consistent result under all five large-scale patterns can be obtained, i.e., the amplitude is larger in the active than the inactive QBWO phase (figure not shown), which corresponds to more (fewer) TCGs over the WNP during the active (inactive) QBWO phase. SSW trains may be an important factor determining the productivity of TCG events over the WNP. Further study is necessary to reveal the detail of the possible link between them, as well as the possible underlying physical mechanism.

4. Summary and conclusions

This paper is an extension of the work of Zhao et al. (2015b); it focuses on investigating the modulation of WNP TCG events by the QBWO, and the association with five large-scale patterns, during the peak TC season for the period 1998–2012. The five flow patterns favorable for WNP TCG events have been illustrated in previous studies (Ritchie and Holland, 1999; Yoshida and Ishikawa, 2013). Following Yoshida and Ishikawa (2013), the five flow patterns, i.e., SL, CF, EW, PTC and GY, are also identified in this study. The results of the present study in this regard are consistent with those of previous studies (Ritchie and Holland, 1999), which suggest that the majority of TCG cases are associated with the SL flow pattern, a moderate number of TCG cases are associated with the CF and EW patterns, and very few TCG events are linked to the PTC and GY patterns. Based on the identification of each large-scale pattern, three of the patterns (i.e. SL, CF and GY) are linked uniquely to monsoonal circulation. Meanwhile, the EW flow pattern is closely associated with enhanced easterly wind from the Central Pacific, and TC cases under the PTC pattern are closely associated with the Rossby wave energy dispersion of previous TCG events.

The modulation of WNP TCG events by the QBWO under different large-scale patterns is investigated by assessing the relative importance of environmental factors. A strong impact of the QBWO on local WNP TCG events is found, with more TCG events forming over the WNP during the active phase compared to the inactive phase. Apart from the PTC pattern, similar results are found for all of the basic patterns. Different from Zhao et al. (2015b), slightly more TCG cases are detected during the inactive phase than during the active phase.

The respective contribution of each factor involved in the GPI is further assessed following previous studies (Jiang et al., 2012; Zhao et al., 2015a, 2015b). During a life cycle of the QBWO, large positive GPI anomalies are spatially correlated with WNP TCG events. Further analyses suggest that the roles of these environmental factors depend largely on the different QBWO phases. During the active QBWO phase, the mid-level relative humidity and low-level relative vorticity are the two most important factors contributing to positive GPI anomalies. Weak contributions are made by the nonlinear and PI terms. These positive contributions are partly offset by the negative contribution from the vertical wind shear term. Contrary to that during the active QBWO phase, the mid-level relative humidity appears to be the only large contributor to positive GPI anomalies during the inactive phase. The positive contribution from the nonlinear term during the inactive phase is slightly higher than the contribution from the low-level relative vorticity, which is distinctly different from the situation during the active phase when the contribution made by the low-level relative vorticity is the second most important. The vertical wind shear term makes a positive contribution to GPI anomalies during the inactive QBWO phase, also different from that during the active phase. These positive contributions are also partly cancelled out by the negative contribution made by the PI term. Almost identical results can be obtained for all of the five large-scale patterns, except GY. For the GY pattern, the total GPI anomalies and the contribution of each linear factor to the GPI anomalies appear to be larger than that for the other four flow patterns. Additionally, the role of vertical wind shear in the composite GPI anomalies for the GY flow pattern is distinct from that obtained without distinguishing the large-scale patterns. These results may partly stem from very few TCGs being associated with the monsoon-related GY pattern over the WNP, but this needs further investigation.

Compared with the results of Zhao et al. (2015b), it is found that the contributions of the four linear terms to the positive GPI anomalies associated with the QBWO are significantly different to those associated with the MJO. First, the contribution of the PI term to GPI anomalies associated with the QBWO (MJO) mode is positive (negative) during the active (inactive) phase of the QBWO (MJO). The contribution from the PI term appears to be out of phase between the MJO and QBWO phases. Second, the contribution of relative vorticity to GPI anomalies is second most important

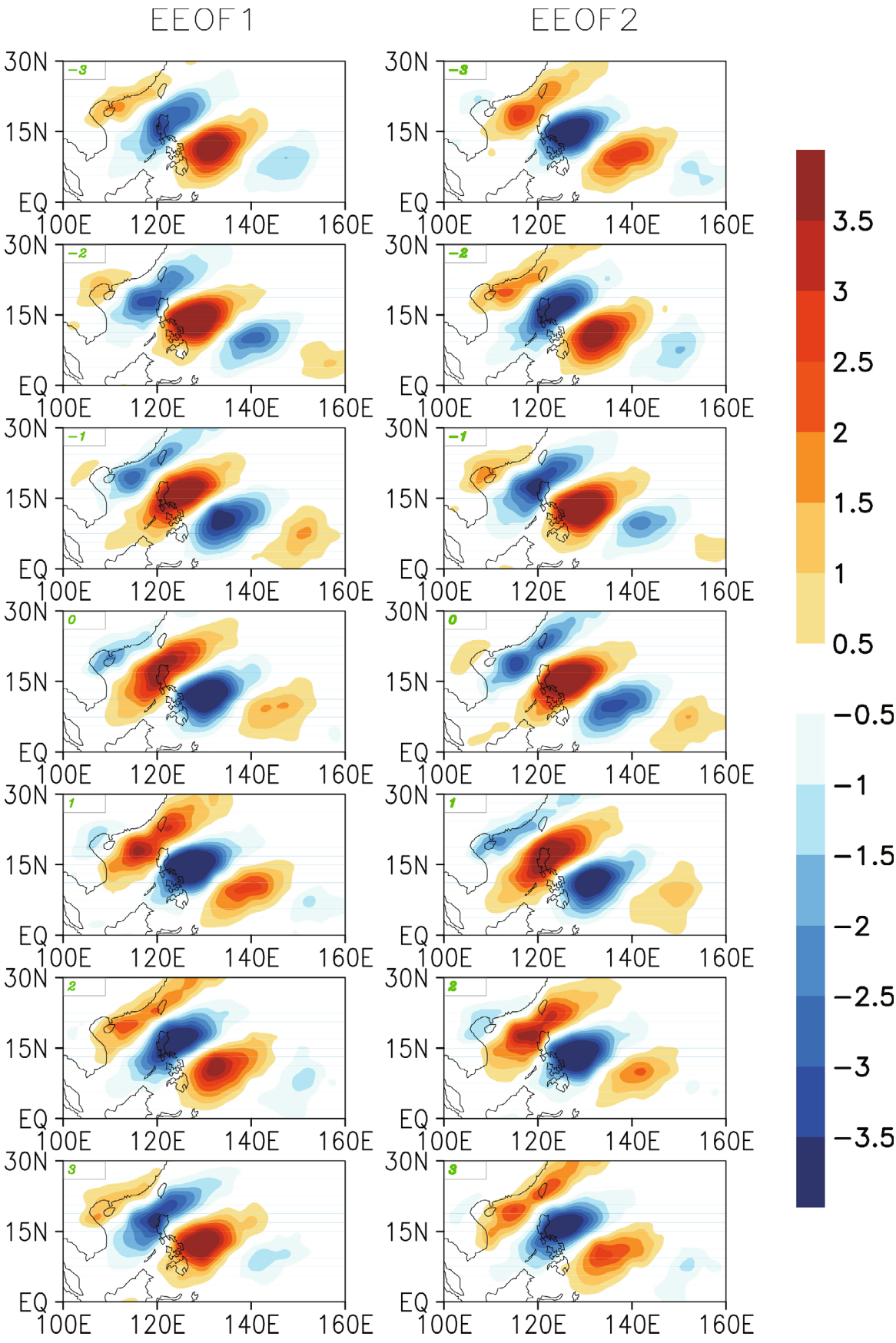

Fig. 11. Evolution of SSW patterns from lag(−3) to lag(+3) days (units: mm d^{-1}).

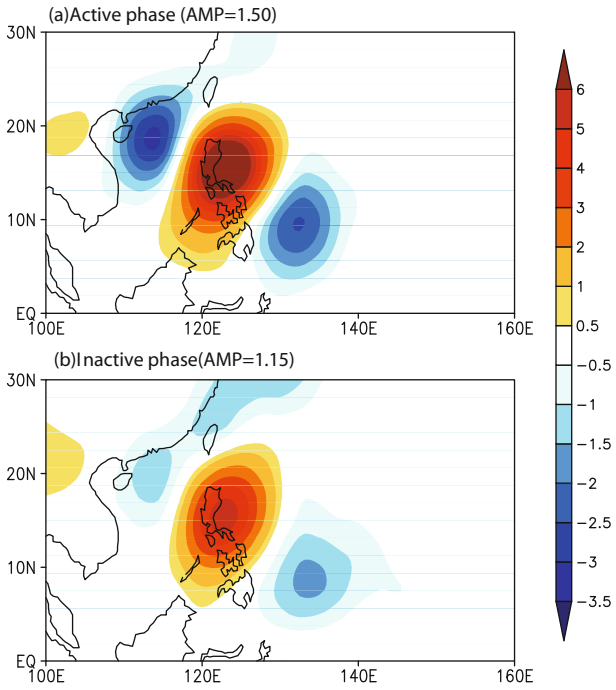

Fig. 12. Spatial patterns of the WNP SSW mode during the (a) active and (b) inactive QBWO phases.

during the MJO inactive phase, whereas its contribution is weak during the QBWO inactive phase. Additionally, the non-linear term (contributing positively towards the positive GPI anomalies) has a relatively similar contribution during the active and inactive phases of the QBWO, different from its impact during the MJO. During the convectively active MJO period, the positive contribution of the nonlinear term tends to be larger than that during the convectively suppressed period. This may be linked to different physical mechanisms being responsible for the modulation of WNP TCG events by the two intraseasonal modes (Zhou and Li, 2010). Note that interactions between SSWs and the low-frequency large-scale oscillations of the QBWO and MJO may lead to changes in GPI anomalies and TCG cases. The relationship between GPI anomalies and TCG cases might be different under the influences of the QBWO and MJO, which is deserving of further investigation.

The possible link between TCG and SSWs over the WNP associated with the QBWO is also investigated. The SSWs are regarded as a major seeding for WNP TCG (Li, 2006; Fu et al., 2007). During the active QBWO phase, the SSW amplitude is larger than that during the inactive phase. The result is valid for all of the large-scale patterns, except GY, and more TCGs occur during the active QBWO phase. In this study, only about 7% of the total 311 TCG events occur under the PTC pattern. Based upon the definition of TC cases associated with the PTC pattern, it is explicitly understood that these TCs correspond to SSWs over the WNP. Similarly, the considerable number of TC cases occurring under other flow patterns might also be closely associated with SSWs. For example, as suggested in previous studies, a mixed Rossby–gravity wave can transit to SSWs in an environment of active convection and zonal wind confluence (Dickinson and Molinari, 2002; Aiyyer and Molinari, 2003), suggesting TCG events under the EW pattern and CF pattern may be associated with SSWs. Thus, the variability of SSWs may bear a close relationship with WNP TCG events. Additionally, a number of studies have suggested that TCG over the WNP basin might also be related with other convectively coupled equatorial waves (Bessafi and Wheeler, 2006; Frank and Roundy, 2006). To date, studies on the equatorial waves and TCs associated with the five major large-scale patterns are relatively limited.

Acknowledgements. This study was jointly supported by the National Natural Science Foundation of China (Grant Nos. 41675072, 41305050, 41275093, 41475091 and 41305039), the National Basic Research Program of China (Grant Nos. 2013CB430301, 2013CB430103 and 2015CB452803), the Jiangsu Provincial Natural Science Fund Project (Grant No. BK20150910), the Natural Science Foundation of the Jiangsu Higher Education Institutions of China (Grant No. 14KJA170005), the Priority Academic Program Development of Jiangsu Higher Education Institutions (PAPD), the Project of Global Change and Air–Sea Interaction (Grant No. GASI-03-IPOVAI-04), and the base funding of the Atlantic Oceanographic and Meteorological Laboratory (AOML). The findings and conclusions in this report are those of the author(s) and do not necessarily represent the views of the funding agency. This study is Earth System Modelling Center Contribution Number 117.

REFERENCES

Aiyyer, A. R., and J. Molinari, 2003: Evolution of mixed Rossby-gravity waves in idealized MJO environments. *J. Atmos. Sci.*, **60**, 2837–2855.

Bessafi, M., and M. C. Wheeler, 2006: Modulation of South Indian Ocean tropical cyclones by the Madden–Julian oscillation and convectively coupled equatorial waves. *Mon. Wea. Rev.*, **134**, 638–656.

Bister, M., and K. A. Emanuel, 2002: Low frequency variability of tropical cyclone potential intensity 1. Interannual to interdecadal variability. *J. Geophys. Res.*, **107**(D24), ACL 26-1–ACL 26-15.

Camargo, S. J., and A. H. Sobel, 2005: Western North Pacific tropical cyclone intensity and ENSO. *J. Climate*, **18**, 2996–3006.

Camargo, S. J., M. C. Wheeler, and A. H. Sobel, 2009: Diagnosis of the MJO modulation of tropical cyclogenesis using an empirical index. *J. Atmos. Sci.*, **66**, 3061–3074.

Chan, J. C. L., 2005: Interannual and interdecadal variations of tropical cyclone activity over the western North Pacific. *Meteor. Atmos. Phys.*, **89**, 143–152.

Chan, J. C. L., 2008: Decadal variations of intense typhoon occurrence in the western North Pacific. *Proc. Roy. Soc. London*, **464**, 249–272.

Chang, C.-P., and G.T.-J. Chen, 1995: Tropical circulations associated with southwest monsoon onset and westerly surges over the South China Sea. *Mon. Wea. Rev.*, **123**(11), 3254–3267.

Chen, G. H., and C. H. Sui, 2010: Characteristics and origin of quasi-biweekly oscillation over the western North Pacific during boreal summer. *J. Geophys. Res.*, **115**(D14), D14113.

Chen, T. C., and J. M. Chen, 1993: The 10–20-day mode of the 1979 Indian monsoon: Its relation with the time variation of monsoon rainfall. *Mon. Wea. Rev*., **121**, 2465–2482.

Chen, T. C., M. C. Yen, and P. S. Weng, 2000: Interaction between the summer monsoons in East Asia and the South China Sea: Intraseasonal monsoon modes. *J. Atmos. Sci*., **57**(9), 1373–1392.

Chia, H.-H, and C.-F. Ropelewski, 2002: The interannual variability in the genesis location of tropical cyclones in the northwest Pacific. *J. Climate*, **15**, 2934–2944.

Dare, R. A., and J. L. McBride, 2011: The threshold sea surface temperature condition for tropical cyclogenesis. *J. Climate*, **24**, 4570–4576.

Dickinson M., J. Molinari, 2002: Mixed Rossby-gravity waves and western Pacific tropical cyclogenesis. Part I: Synoptic evolution. *J. Atmos. Sci*., **59**(14), 2183–2196.

Emanuel, K. A., and D. S. Nolan, 2004: Tropical cyclone activity and the global climate system. *Preprints*, *26th Conf. on Hurricanes and Tropical Meteorology*, Miami, FL, Amer. Meteor. Soc., 10A. 2.

Frank, W. M., and P. E. Roundy, 2006: The role of tropical waves in tropical cyclogenesis. *Mon. Wea. Rev*., **134**, 2397–2417.

Fu, B., T. Li, M. S. Peng, and F. Z. Weng, 2007: Analysis of tropical cyclogenesis in the western North Pacific for 2000 and 2001. *Wea. Forecasting*, **22**, 763–780.

Gray, W. M., 1968: Global view of the origin of tropical disturbances and storms. *Mon. Wea. Rev*., **96**, 669–700.

Gray, W. M., 1979: Hurricanes: Their formation, structure and likely role in the tropical circulation. *Meteorology Over the Tropical Oceans*, D. B. Shaw, Ed., Roy, Meteorological Society, 155–218.

Hartmann D. L., M. L. Michelsen, S. A. Klein, 1992: Seasonal variations of tropical intraseasonal oscillations: A 20-25-day oscillation in the western Pacific. *J. Atmos. Sci*., **49**(14), 1277–1289.

Ho, C. H., J. J. Baik, J. H. Kim, D. Y. Gong, and C. H. Sui, 2004: Interdecadal changes in summertime typhoon tracks. *J. Climate*, **17**(9), 1767–1776.

Hsu, H.-H., C.-H. Weng, and C. H. Wu, 2004: Contrasting characteristics between the northward and eastward propagation of the intraseasonal oscillation during the boreal summer. *J. Climate*, **17**, 727–743.

Huang, P., C. Chou, and R. H. Huang, 2011: Seasonal modulation of tropical intraseasonal oscillations on tropical cyclone geneses in the western North Pacific. *J. Climate*, **24**, 6339–6352.

Huffman, G. J., and Coauthors, 2007: The TRMM multi-satellite precipitation analysis: Quasi-global, multi-year, combined-sensor precipitation estimates at fine scales. *Journal of Hydrometeorology*, **8**, 38–55.

Jiang, X. A., T. Li, and B. Wang, 2004: Structures and mechanisms of the northward propagating boreal summer intraseasonal oscillation. *J. Climate*, **17**, 1022–1039.

Jiang, X. A., M. Zhao, and D. E. Waliser, 2012: Modulation of tropical cyclones over the eastern Pacific by the intraseasonal variability simulated in an AGCM. *J. Climate*, **25**, 6524–6538.

Kim, J. H., C. H. Ho, H. S. Kim, C. H. Sui, and S. K. Park, 2008: Systematic variation of summertime tropical cyclone activity in the western North Pacific in relation to the Madden-Julian oscillation. *J. Climate*, **21**, 1171–1191.

Klotzbach, P. J., 2014: The Madden–Julian Oscillation's impacts on worldwide tropical cyclone activity. *J. Climate*, **27**(6), 2317–2330.

Klotzbach, P. J. and W. M. Gray, 2008: Multidecadal variability in North Atlantic tropical cyclone activity. *J. Climate*, **21**, 3929–3935.

Klotzbach, P. J., and E. C. J. Oliver, 2015: Variations in global tropical cyclone activity and the Madden–Julian oscillation since the midtwentieth Century. *Geophys. Res. Lett*., **42**, 4199-4207, doi: 10.1002/2015GL06396.

Lander, M. A., 1994: An exploratory analysis of the relationship between tropical storm formation in the western North Pacific and ENSO. *Mon. Wea. Rev*., **122**, 636–651.

Lau, K.-H., and N.-C. Lau, 1990: Observed structure and propagation characteristics of tropical summertime synoptic scale disturbances. *Mon. Wea. Rev*., **118**, 1888–1913.

Lee, J.-Y., B. Wang, M. C. Wheeler, X. H. Fu, D. E. Waliser, and I.-S. Kang, 2013: Real-time multivariate indices for the boreal summer intraseasonal oscillation over the Asian summer monsoon region. *Climate Dyn*., **40**, 493–509.

Li, C. Y., and Y. P. Zhou, 1995: On quasi-two-week (10-20-day) oscillation in the tropical atmosphere. *Scientia Atmospherica Sinica*, **19**, 435–444. (in Chinese)

Li, R. C. Y., and W. Zhou, 2013a: Modulation of Western North Pacific tropical cyclone activity by the ISO. Part I: Genesis and intensity. *J. Climate*, **26**, 2904–2918.

Li, R. C. Y., and W. Zhou, 2013b: Modulation of western North Pacific tropical cyclone activity by the ISO. Part II: Tracks and landfalls. *J. Climate*, **26**, 2919–2930.

Li, T., 2006: Origin of the summertime synoptic-scale wave train in the western North Pacific. *J. Atmos. Sci*., **63**, 1093–1102, doi: 10.1175/JAS3676.1.

Li, T., and B. Fu, 2006: Tropical cyclogenesis associated with Rossby wave energy dispersion of a preexisting typhoon. Part I: Satellite data analyses. *J. Atmos. Sci*., **63**, 1377–1389.

Li, T., X. Y. Ge, B. Wang, and Y. T. Zhu, 2006: Tropical cyclogenesis associated with Rossby wave energy dispersion of a preexisting typhoon. Part II: Numerical simulations. *J. Atmos. Sci*., **63**, 1390–1409.

Liebmann, B., H. H. Hendon, and J. D. Glick, 1994: The relationship between tropical cyclones of the western Pacific and Indian Oceans and the Madden–Julian Oscillation. *J. Meteor. Soc. Japan*, **72**, 401–412.

Liu, K. S., and J. C. L. Chan, 2008: Interdecadal variability of western North Pacific tropical cyclone tracks. *J. Climate*, **21**, 4464–4476.

Madden, R. A., and P. R. Julian, 1971: Detection of a 40–50 day oscillation in the zonal wind in the tropical Pacific. *J. Atmos. Sci*., **28**, 702–708.

McBride, J. L., 1981: Observational analysis of tropical cyclone formation. Part III: Budget analysis. *J. Atmos. Sci*., **38**, 1152–1166.

McBride, J. L., R. Zehr, 1981: Observational analysis of tropical cyclone formation. Part II: Comparison of non-developing versus developing systems. *J. Atmos. Sci.*, **38**(6), 1132–1151.

Nakazawa, T., 1986: Intraseasonal variations of OLR in the tropics during the FGGE year. *J. Meteor. Soc. Japan*, **64**, 17–34.

Nakazawa, T., 1988: Tropical super clusters within intraseasonal variations over the Western Pacific. *J. Meteor. Soc. Japan*, **66**, 823–839.

Onogi, K., and Coauthors, 2007: The JRA-25 reanalysis. *J. Meteor. Soc. Japan*, **85**, 369–432.

Reed, R. J., and E. E. Recker, 1971: Structure and properties of synoptic-scale wave disturbances in the equatorial western

Pacific. *J. Atmos. Sci*., **28**, 1117–1133.

Reed, R. J., D. C. Norquist, and E. E. Recker, 1977: The structure and properties of African wave disturbances as observed during phase III of GATE. *Mon. Wea. Rev*., **105**, 317–333.

Ritchie, E. A., and G. J. Holland, 1999: Large-scale patterns associated with tropical cyclogenesis in the western Pacific. *Mon. Wea. Rev*., **127**, 2027–2043.

Sobel, A. H., and C. S. Bretherton, 1999: Development of synoptic-scale disturbances over the summertime tropical northwest Pacific. *J. Atmos. Sci*., **56**, 3106–3127.

Takayabu, N. Y., and T. Nitta, 1993: 3–5 day-period disturbances coupled with convection over the tropical Pacific Ocean, *J. Meteor. Soc. Japan*, **71**, 221–246.

Wang, B., and X. H. Xu, 1997: Northern hemisphere summer monsoon singularities and climatological intraseasonal oscillation. *J. Climate*, **10**(5), 1071–1085.

Wang, B., and J. C. L. Chan, 2002: How strong ENSO events affect tropical storm activity over the western North Pacific. *J. Climate*, **15**, 1643–1658.

Wang, B., and X. Zhou, 2008: Climate variation and prediction of rapid intensification in tropical cyclones in the western North Pacific, *Meteor. Atmos. Phys*., **99**, 1–16, doi: 10.1007/s00703-006-0238-z.

Wang, L., G. H. Chen, and R. H. Huang, 2009: The modulation of quasi-biweekly oscillation on tropical cyclone activity over the western North Pacific. *Chinese Journal of Atmospheric Sciences*, **33**, 416–424. (in Chinese)

Wheeler, M. C., and H. H. Hendon, 2004: An all-season real-time multivariate MJO index: Development of an index for monitoring and prediction. *Mon. Wea. Rev*., **132**, 1917–1932.

Wu, L., J. Liang, and C.-C. Wu, 2011: Monsoonal Influence on Typhoon Morakot (2009). Part I: Observational Analysis. *J. Atmos. Sci.*, **68**, 2208–2221.

Wu, L., and J. Duan, 2015: Extended simulation of tropical cyclone formation in the western North Pacific monsoon trough. *J. Atmos. Sci.*, **72**, 4469–4485.

Yasunari, T., 1979: Cloudiness fluctuations associated with the northern hemisphere summer monsoon. *J. Meteor. Soc. Japan*, **57**, 227–242.

Yoshida, R., and H. Ishikawa, 2013: Environmental factors contributing to tropical cyclone genesis over the western North Pacific. *Mon. Wea. Rev*., **141**, 451–467.

Yoshida, R., Y. Kajikawa, and H. Ishikawa, 2014: Impact of boreal summer intraseasonal oscillation on environment of tropical cyclone genesis over the Western North Pacific. *SOLA*, **10**, 15–18.

Zhang, Q., Q. Liu, and L. Q. Wu, 2009: Tropical cyclone damages in China 1983–2006. *Bull. Amer. Meteor. Soc*., **90**, 489–495.

Zhao, H. K., and L. G. Wu, 2014: Inter-decadal shift of the prevailing tropical cyclone tracks over the western North Pacific and its mechanism study. *Meteor. Atmos. Phys*., **125**, 89–101.

Zhao, H. K., and C. Z. Wang, 2015: Interdecadal modulation on the relationship between ENSO and typhoon activity during the late season in the Western North Pacific. *Climate Dyn*., doi: 10.1007/s00382-015-2837-1.

Zhao, H. K., L. G. Wu, and W. C. Zhou, 2010: Assessing the influence of the ENSO on tropical cyclone prevailing tracks in the western North Pacific. *Adv. Atmos. Sci*., **27**(6), 1361–1371, doi: 10.1007/s00376-010-9161-9.

Zhao, H. K., L. G. Wu, and W. C. Zhou, 2011: Interannual changes of tropical cyclone intensity in the western north Pacific. *J. Meteor. Soc. Japan*, **89**(3), 243–253, doi: 10.2151/jmsj.2011-305.

Zhao, H. K., L. G. Wu, and R. F. Wang, 2014: Decadal variations of intense tropical cyclones over the western North Pacific during 1948-2010. *Adv. Atmos. Sci*., **31**(1), 57–65, doi: 10.1007/s00376-013-3011-5.

Zhao, H. K., X. A. Jiang, and L. G. Wu, 2015a: Modulation of Northwest Pacific tropical cyclone genesis by the intraseasonal variability. *J. Meteor. Soc. Japan*, **93**(1), 81–97, doi: 10.2151/jmsj.2015-006.

Zhao, H. K., R. Yoshida, and G. B. Raga, 2015b: Impact of the madden-Julian oscillation on Western North Pacific tropical cyclogenesis associated with large-scale patterns. *Journal of Applied Meteorology and Climatology*, **54**, 1423–1429, doi: 10.1175/JAMC-D-14-0254.1.

Zhao, H. K., X. A. Jiang, and L. G. Wu, 2016: Boreal summer synoptic-scale waves over the western North Pacific in multimodel simulations. *J. Climate*, doi: 10.1175/JCLI-D-15-0696.

Zhou, C. H., and T. Li, 2010: Upscale feedback of tropical synoptic variability to intraseasonal oscillations through the nonlinear rectification of the surface latent heat flux. *J. Climate*, **23**, 5738–5754.